Original Research

Core Ideas

- A new thermo-TDR sensor can determine soil thermal properties, water content, bulk density, porosity, and air-filled porosity.
- The new theories are used to analyze the heat-pulse data and TDR waveforms.
- The new sensor provides greater sensing volume and more accurate results than previous designs.

W. Peng, Y. Lu, X. Xie, and T. Ren, College of Resources and Environmental Sciences, China Agricultural Univ., Beijing, China 100193; R. Horton, Dep. of Agronomy, Iowa State Univ., Ames, IA 50011. *Corresponding author (luyili@cau.edu.cn).

An Improved Thermo-TDR Technique for Monitoring Soil Thermal Properties, Water Content, Bulk Density, and Porosity

Wei Peng, Yili Lu,* Xiaoting Xie, Tusheng Ren, and Robert Horton

The thermo-time domain reflectometry (thermo-TDR) technique is valuable for monitoring in situ soil water content (θ), thermal properties, bulk density (ρ_b), porosity (n), and air-filled porosity (n_a) in the vadose zone. However, the previous thermo-TDR sensor has several weaknesses, including limited precision of TDR waveforms due to the short probe length, small measurement volume, and thermal property estimation errors resulting from finite probe properties not accounted for by the heat pulse method. We have developed a new thermo-TDR sensor design for monitoring θ, thermal properties, ρ_b, n, and n_a. The new sensor has a robust heater probe (outer diameter of 2.38 mm and length of 70 mm) and a 10-mm spacing between the heater and sensing probes, which provides a sensing volume three times larger than that of the previous sensor. The identical cylindrical perfect conductors and the tangent line–second-order bounded mean oscillation theories were applied to analyze the raw data. Laboratory tests showed that θ values determined with the new sensor had a RMSE of 0.014 m^3 m^{-3} compared with 0.016 to 0.026 m^3 m^{-3} with the previous sensor. Soil thermal property estimates with the new sensor agreed well with modeled values. Soil ρ_b, n, and n_a derived from θ and thermal properties were consistent with those derived from gravimetric measurements. Thus, the new thermo-TDR sensor provides more accurate θ, thermal properties, ρ_b, n, and n_a values than the previous sensor.

Abbreviations: ICPC, identical cylindrical perfect conductors; ILS, infinite line source; TDR, time domain reflectometry; TL-BMO, tangent line–second-order bounded mean oscillation.

Dynamic measurements of soil temperature, water content (θ), and thermal properties are necessary for a quantitative description of soil coupled heat and water transfer. From simultaneous measurements of θ and thermal properties, additional soil properties and processes can be determined, including bulk density (ρ_b), porosity (n), air-filled porosity (n_a), degree of water saturation (Ochsner et al., 2001a; Ren et al., 2003a; Liu et al., 2014), soil water evaporation (Zhang et al., 2012), soil heat flux (Peng et al., 2017), unsaturated hydraulic conductivity of the surface soil (Tian et al., 2018), and water flux density (Ren et al., 2000; Mori et al., 2003; Kamai et al., 2008). Among the existing techniques, the thermo-time domain reflectometry (thermo-TDR) sensor, which consists of three parallel probes with 40-mm length (L), 1.3-mm diameter (d), and 6-mm probe-to-probe spacing (r), can measure soil temperature, θ, and thermal and electrical properties on a soil volume (Ren et al., 1999, 2005). The sensor has been used widely in monitoring soil physical properties (Ochsner et al., 2001b; Lu et al., 2007, 2014; Xie et al., 2018), and in studying coupled heat and water transfer in unfrozen and frozen soils (Heitman et al., 2008; Tian et al., 2015).

The small sensing volume of the thermo-TDR design makes it suitable for fine-scale measurements, but in some cases restricts the representativeness of actual field conditions. In addition, short probes can limit the accuracy and precision of TDR measurements (Noborio, 2001; Schwartz et al., 2014; Wang et al., 2015). Topp et al. (1984) reported that the errors in TDR θ with a 0.05-m-long probe were significant, with a standard deviation of 0.037 m^3 m^{-3}, while an improved accuracy was observed for sensors with longer probes.

Several studies have been performed to improve the accuracy of thermo-TDR sensors for determining soil thermal properties. Olmanson and Ochsner (2008) developed a partial cylinder-shaped thermo-TDR sensor that had curved heaters and a central temperature probe. The sensor was almost twice the size of the Ren et al. (1999) sensor. This design enhanced the strength and robustness of the sensor, but it introduced other errors such as soil compaction caused by the curved heater (Olmanson and Ochsner, 2008). Liu et al. (2008) improved the original Ren et al. (1999) sensor design by adding pointed tips to the probe ends, increasing the probe d to 2 mm and r to 8 mm. The pointed tips improved the ease of sensor insertion into soil, but the short probe L still limited its measurement accuracy. A similar design proposed by Yu et al. (2015) had pointed probe tips, 2-mm d, 40.5-mm L, and 6-mm r. Wen et al. (2018) increased L to 60 mm with temperature sensors positioned at multiple locations in the sensing probes, which allowed in situ self-corrections of changes in r due to probe deflection. They also reported that the longer probes significantly increased the accuracy of TDR θ results.

In recent years, improved theories have been put forward to calculate thermal properties and θ. Knight et al. (2012) identified errors due to finite probe properties that were ignored in the infinite line source (ILS) model. They proposed the identical cylindrical perfect conductors (ICPC) model to improve estimations of soil thermal properties by accounting for finite probe heat capacity and finite probe radius. Kamai et al. (2015) showed that errors in soil heat capacity (C) estimations were reduced significantly by using a large heater probe (d = 2.38 mm) with a thick tubing wall and adoption of the ICPC theory. Wang et al. (2015) proposed a tangent line/second-order bounded mean oscillation (TL-BMO) approach to determine the reflection positions of TDR waveforms, which increased the accuracy of the relative dielectric permittivity (K_a) and θ results. However, these theories have not been fully integrated into the thermo-TDR system.

It is desirable to develop a more robust and accurate sensor that overcomes the limitations of conventional ILS theory, small sampling volumes, and thin probes of the previous thermo-TDR sensors. The objective of this study was to develop and test a new thermo-TDR sensor design with a sampling volume larger than that of the previous thermo-TDR sensor. Determinations of θ, thermal properties, ρ_b, n, and n_a with the new sensor were tested under laboratory conditions.

⬧New Sensor Design
Thermo-TDR Sensor Design Criteria

The design criteria of thermo-TDR sensors were introduced by Ren et al. (1999), who showed that L, d, and r were the three major sensor design factors affecting heat pulse and TDR measurements. For a TDR waveguide, a small d (compared with r) affects the electromagnetic field distribution around the probes, and any local nonuniformity around the sensor can impact θ measurements, while a large d may cause soil compaction and disturbance

(Ghezzehei, 2008). Knight(1992) suggested that r/d should be <10. Meanwhile, waveforms generated by short sensors are prone to errors resulting from multiple superimposed reflections (Wang et al., 2015, 2017). With longer TDR sensors, the position of the second reflection point is more identifiable and stable, resulting in more reliable TDR θ results (Noborio, 2001; Schwartz et al., 2014).

The heat pulse sensor configuration also requires an appropriate sensor size for accurate soil thermal property estimations. For example, to limit the axial heat flow error to <1%, Blackwell (1956) suggested that the ratio of L to d should be >25 for the single-probe method to determine soil thermal conductivity (λ). To limit the relative errors for C and thermal diffusivity (κ) to <2%, Kluitenberg et al. (1995) suggested that $L/2r > 2.2$ and $d/2r < 0.13$, with the purpose of reducing the ILS model errors caused by the finite sensor size associated with the dual-probe heat pulse senor. It should be noted that the analysis of Blackwell (1956) and Kluitenberg et al. (1995) considered the heater probe as a line heat source.

The New Thermo-TDR Sensor

We propose a new thermo-TDR sensor design by including a relatively large heater to reduce probe deflections during sensor insertion into the soil, a relatively large L to improve the accuracy of TDR θ measurements, and a relatively large r to satisfy the design criteria. Figure 1 depicts the details of the new thermo-TDR sensor. Compared with the original design of Ren et al. (1999), the main changes incorporated in the new sensor are: (i) L is increased to 70 mm; (ii) the heating probe is larger and more rigid (2.38-mm outer diameter and 0.71-mm wall thickness); (iii) the sensing probes are larger and more rigid (2-mm outer diameter and 0.25-mm wall thickness); (iv) r is increased to 10 mm, and three thermocouples (chromel-constantan, 40 American wire gauge [AWG]) are enclosed in each sensing probe, located at 20, 35, and 50 mm away from the sensor base.

The probes are made of stainless steel tubes with pointed tips. The resistance heater wire is made of 38-gauge Nichrome 80 wire (two loops). Both the heater wire and thermocouples are kept in place with high-thermal-conductivity epoxy, which also serves to provide water resistance and electrical insulation. A coaxial cable is connected to the sensor by soldering the inner conductor to the central probe and the shield to the outer probes. A casting epoxy resin (CR-600, Micro-Mark) is used to fix each part in place in the sensor head (Fig. 1). He et al. (2018) provided additional sensor construction insights.

⬧Materials and Methods
Sensing Volume of the New Thermo-TDR Sensor

A simple experiment, which used distilled water at 20°C as the medium, was performed to determine the approximate TDR measurement volume of the new sensor. The schematic diagram for the experiment setup can be found in Supplemental Fig. S1.

A thermo-TDR sensor was placed in a rectangular glass container (16-cm width, 8-cm height, and 22.5-cm length) in such a
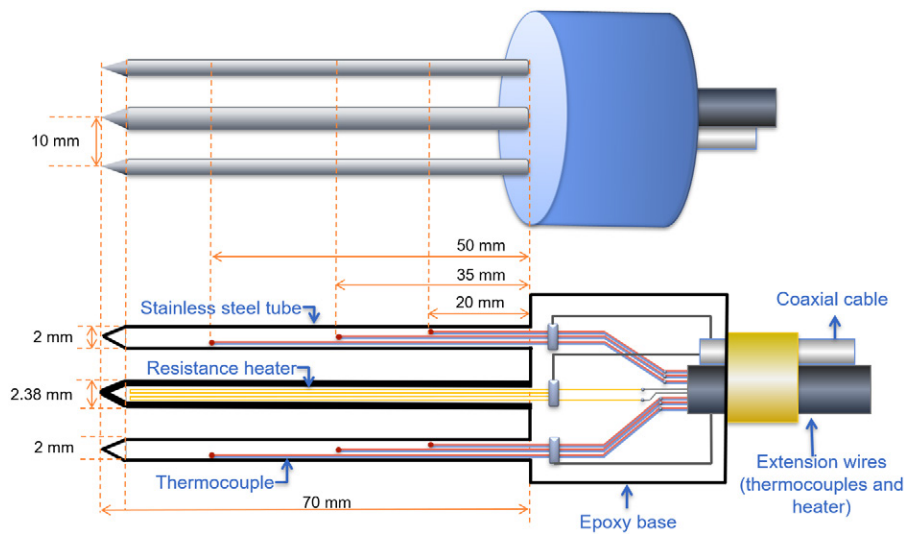
Fig. 1. A schematic diagram showing the design of the new thermo-TDR sensor. The drawing is not to scale.

way that all three probes were laterally arranged so that the probe plane was parallel to the container bottom and the outer probes were at the same height as the central probe (Supplemental Fig. S1a). Distilled water was initially added to the container to a level just above the probe plane; additional water was added in 2-mm increments, with TDR waveforms collected after each increment. In another case, a thermo-TDR sensor was placed in the container with the longitudinal arrangement for the probes so that the probe plane was vertical to the container bottom and the outer probes were above and below the central probe (Supplemental Fig. S1b). Distilled water was initially added to the container to a level just above the central probe; additional water was added in 2-mm increments, with TDR waveforms collected after each increment. The water-filling process ceased when no changes in the TDR waveforms were observed.

The zones of greatest energy have an elliptical shape (Robinson et al., 2003). From the above measurements, we determined the long axis and short axis of the elliptical measurement range or the maximum detectable boundaries of the TDR sensor (Ren et al., 2005).

Measurements on Disturbed and Intact Soil Samples

Both disturbed and intact soil samples were used in this study. The textures of the disturbed soil samples ranged from sand to silt loam. Soil samples were air dried, crushed, and sieved through a 2-mm screen before being used for measurements. The intact soil samples were obtained at the Experimental Farm of China Agricultural University, Beijing, China. Soil samples were collected from the surface layer (0–8 cm) of a field plot using a cutting ring (70-mm inner diameter and 80 mm long). Soil particle-size distributions were measured with the pipette method (Gee and Or, 2002). The physical properties of the soil samples are listed in Table 1.

The apparent L and r of the thermo-TDR sensors were determined using agar-immobilized water (5 g L^{-1}) at 20°C. For details on thermo-TDR sensor calibrations, see Lu et al. (2017). Sieved soil samples were moistened to seven θ values (0, 0.05, 0.10, 0.15, 0.20,

0.25, and 0.30 m^3 m^{-3}) and then packed into cylinders (70-mm inner diameter and 80 mm long) at known ρ_b (Table 1). After equilibration at room temperature, a thermo-TDR sensor was inserted into the soil columns vertically to measure θ and thermal properties. For TDR measurements, the waveforms were recorded with a TDR200 reflectometer device (Campbell Scientific). A constant current of 0.23 A was applied to the central heater for 25 to 30 s to generate the heat pulse, which was controlled with a datalogger (CR3000, Campbell Scientific). The temperature changes at the sensing probes were collected at 1-s intervals for 480 s. Five repeated heat-pulse determinations were taken on each soil column at 60-min intervals. Finally, θ and ρ_b values were determined by oven drying the samples at 105°C for 24 h. These values were used as reference values to evaluate the accuracy of the θ and ρ_b values derived from the new thermo-TDR sensor measurements.

Determination of Soil Thermal Properties Based on Identical Cylindrical Perfect Conductors Theory

The pulsed ILS model has been used widely for calculating thermal properties from heat pulse data (Bristow et al., 1994). The

Table 1. Soil texture, particle size distribution, and bulk density (ρ_b) for the studied soils. Soils 1 to 4 are disturbed samples, and Soils 5 to 7 are intact soil core samples.

Soil no.	Texture	Particle size distribution			ρ_b
		2–0.05 mm	0.05–0.002 mm	<0.002 mm	
		——————— % ———————			Mg m^{-3}
1	sand	94	1	5	1.50–1.68
2	loamy sand	80	12	8	1.41–1.47
3	loam	48	38	14	1.19–1.35
4	silt loam	15	67	18	1.30–1.58
5	loam	52	36	12	1.07–1.54
6	loam	40	48	12	1.07–1.54
7	silt loam	34	53	13	1.07–1.54

model assumes that heat is conducted from an infinite line heat source into a homogeneous, isotropic medium of infinite extent (Kamai et al., 2015). In practice, however, the sensor probes have finite d and L and have thermal properties that differ considerably from those of soils (Knight et al., 2012). The ICPC theory, which accounts for the finite probe radius and finite probe heat capacity, has been shown to provide relatively accurate soil thermal property determinations (Knight et al., 2012; Lu et al., 2013; Kamai et al., 2015). The ICPC model begins with a Laplace-domain solution that represents the case where heat is released continuously at a rate of q' (Knight et al., 2012):

$$\hat{T}_c(p) = \frac{q' K_0(\mu L)}{2\pi\lambda p \left\{ \mu a_0 \left[K_1(\mu a_0) + (\mu a_0 \beta_0/2) K_0(\mu a_0) \right] \right\}^2} \quad [1]$$

where p is the Laplace transform parameter and $\hat{T}_c(p)$ is the Laplace transform of $T_c(t)$, which is the temperature increase with time for the case of continuous heating; $\mu = \sqrt{(p/\kappa)}$, $\beta_0 = C_0/C$, and $K_u(z)$ denotes the modified Bessel function of the second kind of order u and argument z. The radius (a_0) and volumetric heat capacity (C_0) of the heater probe must be known when using Eq. [1]. Equation [1] can be numerically inverted using the Stehfest algorithm to solve for $T_c(t)$ and $T_c(t - t_0)$ for the conditions of the pulsed heating scheme. Details regarding the numerical inversion can be found in Knight et al. (2012). Thus, the temperature in the sensing probe, $T(t)$, can be expressed using

$$T(t) = \begin{cases} T_c(t); & 0 < t \le t_0 \\ T_c(t) - T_c(t - t_0); & t > t_0 \end{cases} \quad [2]$$

Equations [1] and [2] represent the ICPC solution (Knight et al., 2012). Here, the values for a_0 and C_0 are 1.19 mm and 3.68 MJ m^{-3} K^{-1}, respectively (Supplemental Table S1). Based on the ICPC model, soil C and κ were determined by fitting Eq. [1] and [2] to heat pulse sensor measured temperature changes as a function of time, $T(t)$. A MATLAB (The Mathworks) program was used to perform the curve-fitting. Soil λ was calculated as the product of C and κ.

The typical temperature response data obtained in this study and the curve-fitting results are presented in Supplemental Fig. S2 and S3 for the sand soil (at θ of 0 and 0.25 m^3 m^{-3}) and the agar solution. The parameters involved in the curve-fitting process are listed in Supplemental Table S1. It is worth noting that the time range of the temperature change data used for curve fitting depends on the shape of the temperature response curves (Supplemental Table S1).

Determination of TDR Water Content Using the Tangent Line–Second-Order Bounded Mean Oscillation Method

The TL-BMO method can be used to determine the reflection positions in TDR waveforms (Wang et al., 2015). It is a prediction-correction model based on a combination of the tangent line method and the second-order BMO method. The tangent line method is used to approximate the second reflection position (t_2) of a TDR waveform to establish a prediction interval, then the second-order BMO is applied to the same TDR waveform, and the local maximum of the second-order BMO curve within the prediction interval is selected as t_2. The first reflection position (t_1) is unaffected by the probe length.

Once t_1 and t_2 are determined, K_a is estimated, and θ is determined from K_a with (Topp et al., 1980)

$$\theta = 2.92\times10^{-2} K_a - 5.5\times10^{-4} K_a^2 + 4.3\times10^{-6} K_a^3 - 5.3\times10^{-2} \quad [3]$$

Determination of Soil Bulk Density and Porosity Using the Combination of Heat Capacity and Thermal Conductivity Based Methods

We used both C-based and λ-based methods to estimate ρ_b from thermo-TDR measured θ, C, and λ. The C-based method is based on the mixing model of Campbell (1985):

$$\rho_b = \frac{C - c_w \rho_w \theta}{c_s} \quad [4]$$

where ρ_w (1.0 Mg m^{-3}) and c_w (4.18 kJ kg^{-1} K^{-1}) are the density and specific heat capacity of water, respectively, and c_s represents the specific heat capacity of the soil solids. Wang et al. (2019) reported c_s values on nine mineral soils using a differential calorimetry method considering drying temperature and organic matter and clay contents (their Table 3). Based on their published values, we obtained an average c_s value of 0.742 kJ kg^{-1} K^{-1} for soils with an organic matter content <3% and clay content <30%. For soils with either >3% organic matter or 30% clay, an average c_s value of 0.768 kJ kg^{-1} K^{-1} is obtained. Here, we used 0.742 kJ kg^{-1} K^{-1} as the c_s value for all soils in this study.

Lu et al. (2016) introduced the λ-based method for estimating ρ_b from measurements of θ and λ with known soil texture information. The empirical equation that relates λ to ρ_b, θ, and soil particle-size information is (Lu et al., 2016)

$$\lambda = \lambda_{dry} + \exp\left(\beta - \theta^{-\alpha}\right) \quad [5]$$

where α and β are shape factors determined by soil particle sizes and ρ_b:

$$\alpha = 0.67 f_{cl} + 0.24 \quad [6]$$

$$\beta = 1.97 f_{sa} + 1.87 \rho_b - 1.36 f_{sa}\rho_b - 0.95 \quad [7]$$

where f_{sa} and f_{cl} are the mass fractions of sand and clay from the USDA soil texture classification system. The thermal conductivity of a dry soil, λ_{dry} (W m^{-1} K^{-1}), is calculated as (Lu et al., 2016)

$$\lambda_{dry} = -0.56\left(1 - \frac{\rho_b}{2.65}\right) + 0.51 \quad [8]$$

where 2.65 (Mg m^{-3}) is the soil particle density.

Finally, ρ_b is inversely estimated with the least-squares method by fitting Eq. [5–8] to the thermo-TDR measured θ and λ, and n and n_a are calculated as

$$n = 1 - \frac{\rho_b}{\rho_s} \qquad [9]$$

$$n_a = n - \theta \qquad [10]$$

Compared with the C-based method, the λ-based method has the advantage that the λ results are not affected by probe deflection errors (Lu et al., 2016; Tian et al., 2018). However, sensitivity analysis has shown that the λ-based method gives unstable results when θ is lower than a critical water content (Tian et al., 2018; Lu et al., 2018). In this study, we combined the C- and λ-based methods for estimating ρ_b, using the λ-based method at $\theta > 0.1$ m^3 m^{-3} and the C-based method at $\theta \leq 0.1$ m^3 m^{-3}.

Supplemental Fig. S4 presents an overview of the thermo-TDR technique for determining soil physical properties. Briefly, three steps are needed to complete the process. First, a temperature change–time curve is obtained by applying a heat pulse to the soil sample, and a TDR waveform (the voltage or reflection coefficient as a function of time) is generated by launching a fast-rise electromagnetic pulse. Second, soil thermal properties (C and λ) are derived from the temperature curve following the ICPC theory, and K_a is calculated from the TDR waveform using the TL-BMO algorithm, from which θ is determined with Eq. [3]. Finally, ρ_b is estimated from θ, C, or λ with Eq. [4–8], and n and n_a are calculated with Eq. [9] and [10].

Estimation of Thermal Properties Using Existing Models

The performance of the new thermo-TDR sensor was evaluated by comparing the measured thermal property values with model estimates. The de Vries (1963) model, Xie et al. (2018) model, and Lu et al. (2014) model were used to estimate C, κ, and λ, respectively. Model inputs included ρ_b, θ, f_{sa}, and f_{cl}.

The accuracy of the new thermo-TDR sensor determinations was evaluated using root mean square error (RMSE) and bias:

$$\mathrm{RMSE} = \sqrt{\frac{\sum (A_d - A_e)^2}{m}} \qquad [11]$$

$$\mathrm{bias} = \frac{\sum (A_d - A_e)}{m} \qquad [12]$$

where m is the number of data points. For thermal properties (C, κ, λ), A_d represents the sensor value and A_e represents the model value. For θ, ρ_b, n, and

n_a, A_d and A_e represent the values determined by the thermo-TDR sensor and the oven drying method, respectively.

⬥Results and Discussion
Sensing Volume of the New Sensor

Figure 2 shows the recorded TDR waveforms obtained at different water levels above the central probe in the vertical and horizontal plane directions with respect to the container bottom. Because the electromagnetic energy concentrates around the central probe, the greater the distance away from the central probe, the less the electromagnetic energy and the smaller the influence on the TDR waveform (Knight, 1992). When the water–air interface was just on the probe plane, the apparent distance of the TDR waveform was quite small. With further increases in water level, the TDR waveform became wider as the second reflection position grew larger. A full waveform was not obtained until the magnitude of K_a approached the dielectric permittivity value of water. At that point, the outer boundary of the TDR measurement was about 9 mm when the probe plane was parallel to the container
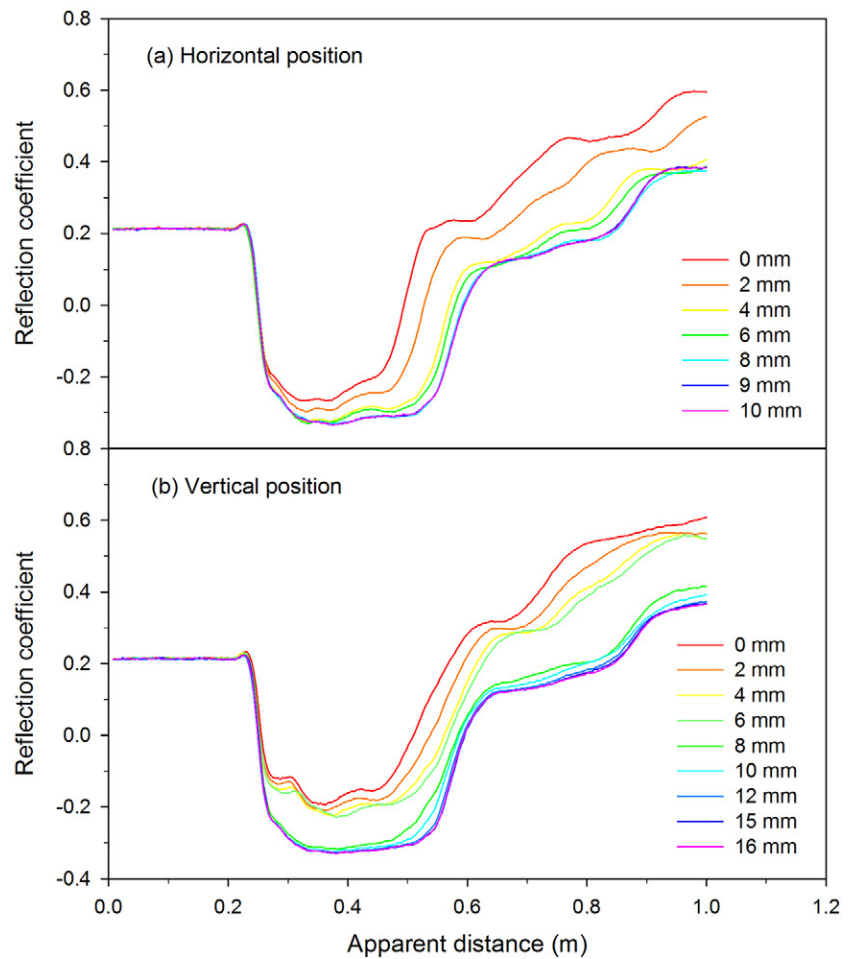

Fig. 2. Thermo-time domain reflectometry (TDR) measured TDR waveforms (apparent distance vs. reflection coefficient) at various water levels under two scenarios: (a) the probe plane is parallel to the container bottom (horizontal position), and (b) the probe plane is vertical to the container bottom (vertical position). A diagram of the experiment setup is provided in Supplemental Fig. S1.

bottom (Fig. 2a) and 15 mm when the probe plane was vertical to the container bottom (Fig. 2b). Thus, the new thermo-TDR sensor measures an elliptical cylindrical shape with a short axis of 9 mm and long axis of 15 mm. The volume of the TDR measurement, 29.7 cm^3, is almost three times that of the Ren et al. (1999) sensor.

According to Knight et al. (2007), the effective measurement outer boundary (which contains 99% of the total spatial sensitivity) of a heat pulse sensor is close to an ellipse with a major axis 2.6 times the probe-to-probe spacing. Thus, the Ren et al. (1999) thermo-TDR sensor has a major axis of 20.8 mm, while the corresponding value is 26 mm for the new thermo-TDR sensor. Therefore, the sampling volume of the new sensor for both heat pulse and TDR measurements is larger than that of the previous sensor.

Soil Thermal Property Values Determined with the New Thermo-TDR Sensor

Figure 3 compares the C, κ, and λ values derived from the new thermo-TDR sensor with the values estimated with the de Vries (1963) C model, the Xie et al. (2018) κ model, and the Lu et al. (2014) λ model, respectively. Each data point represents the mean of measurements from two outer probes (i.e., mean of six values). In the case of probe deflections during the experiment, the Liu et al. (2013) spacing-correction method was used to correct r in situ based on the temperatures measured by the six thermocouples in the two sensing probes. During our measurements, there was very little change in r, possibly due to the rigidity of the probes. Thus, the soil thermal property values derived from all six thermocouples were averaged.

Previous studies have indicated that a heat pulse sensor could overestimate the actual C, especially for relatively dry soils (Tarara and Ham, 1997; Ren et al., 2003b; Knight et al., 2012; Lu et al., 2013). The ILS model has been reported to overestimate C by 5.2% (Ren et al., 2003b) or even by 6.4% on dry soils (Knight et al., 2012). In this study, using the ICPC model, the average C error was about 3% in the θ range of 0 to 0.3 m^3 m^{-3}. The de Vries (1963)

model estimates of C vs. the heat-pulse C values were distributed randomly around the 1:1 line, mostly within the $\pm 10\%$ error lines (Fig. 3a).

The heat pulse κ values vs. the Xie et al. (2018) modeled estimates were generally within the $\pm 10\%$ error lines (Fig. 3b). The few outliners might be due to non-uniformities in the soil cores. The heat pulse λ values vs. the Lu et al. (2014) model estimates were consistent, with nearly all values within the $\pm 10\%$ error lines (Fig. 3c). Thus, by using the ICPC theory, the new thermo-TDR sensor is able to avoid the overestimation errors in C values and underestimation errors in κ values associated with the previous sensors.

Heat Pulse Derived vs. TDR Derived Water Content

Figure 4 presents thermo-TDR sensor derived θ values (θ_{TDR}) vs. θ values determined by oven drying soil samples. The data points are distributed around the 1:1 line, and a linear regression fit to the points had a coefficient of determination (R^2) of 0.980. Compared with oven-dried θ values, the θ_{TDR} values had a RMSE of 0.014 m^3 m^{-3} and a bias of -0.004 m^3 m^{-3}, suggesting that the new sensor provided accurate TDR θ values. This is a significant improvement over the accuracy of the previous thermo-TDR sensors, which was within 0.016 to 0.026 m^3 m^{-3} of the actual θ values (Ren et al., 2003a; Liu et al., 2008; Wen et al., 2018).

Soil water content can also be estimated with heat pulse sensor estimates of C (θ_{HP}, Eq. [4]). Previous work concluded that this method was more appropriate for determining changes in θ rather than in actual values of θ (Basinger et al., 2003; Knight et al., 2012; Lu et al., 2013). Overestimation of θ_{HP} from actual θ were reported to be mostly within a range of 0.026 to 0.067 m^3 m^{-3} (Tarara and Ham, 1997; Song et al., 1998, 1999; Ren et al., 2003b; Lu et al., 2013). Figure 5 shows the results of θ_{HP} determined with the new thermo-TDR sensor vs. oven-dried θ values. In general, the θ values agreed well, as indicated by the random distribution of data points around the 1:1 line and an R^2 value of 0.961 for the correlation between θ_{HP} and θ. Averaged across seven soils, the
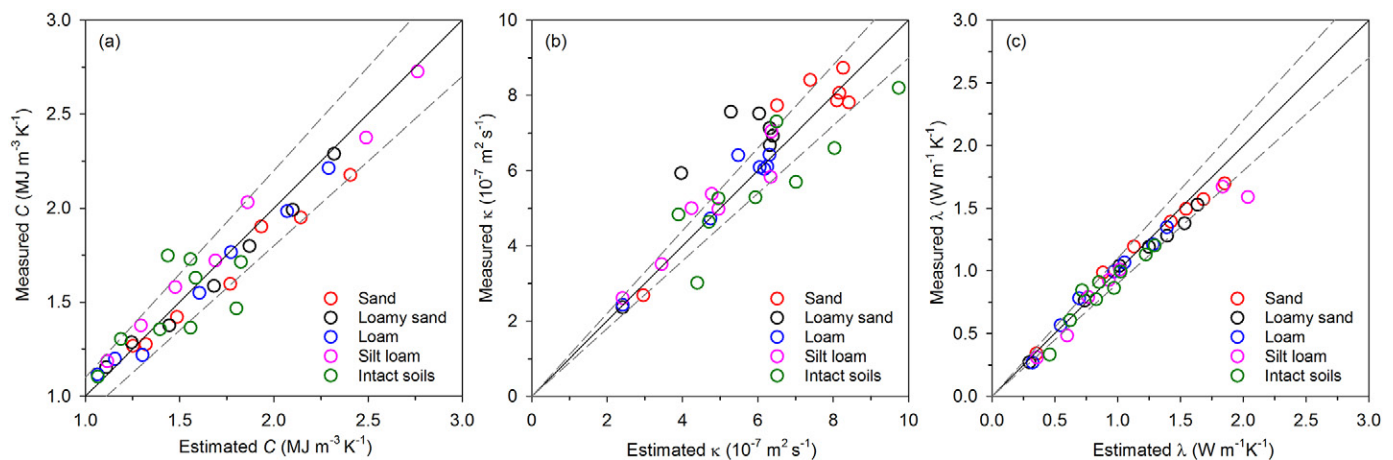

Fig. 3. Comparison of thermo-time domain reflectometry measured thermal properties and model values on disturbed and intact soil samples: (a) measured heat capacity (C) vs. C estimated with the de Vries (1963) model, (b) measured thermal diffusivity (κ) vs. κ estimated with the Xie et al. (2018) model, and (c) measured thermal conductivity (λ) vs. λ estimated with the Lu et al. (2014) model. The solid line is the 1:1 line and the dashed lines are $\pm 10\%$ error lines.
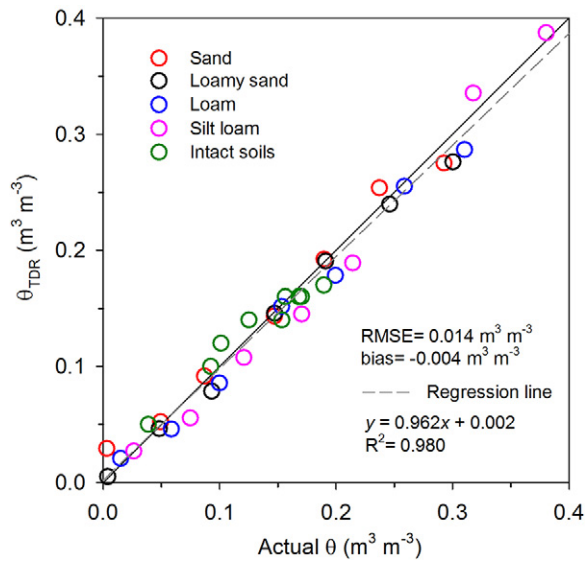
Fig. 4. Comparison of time domain reflectometry (TDR) derived water content (θ_{TDR}) vs. actual values by oven drying samples. The solid line is the 1:1 line and the dashed line is the linear regression line.
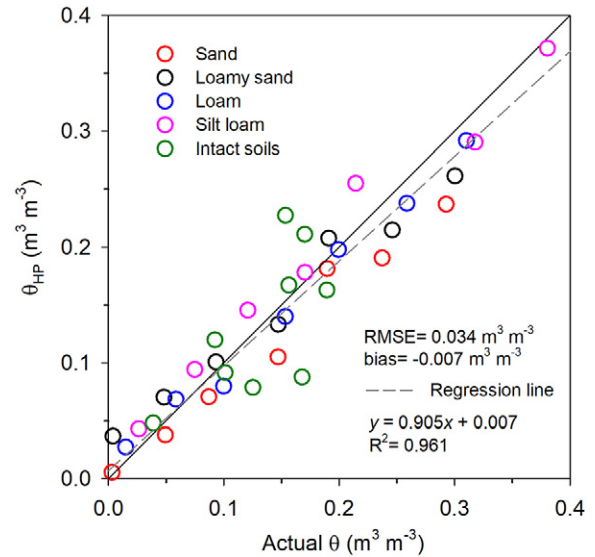

Fig. 5. Heat pulse derived water content (θ_{HP}) vs. actual water content (θ) by oven drying samples. The solid line is the 1:1 line and the dashed line is the linear regression line.

RMSE and bias of θ_{HP} from the ICPC model were 0.034 m^3 m^{-3} and -0.007 m^3 m^{-3}, respectively, lower than the corresponding RMSE (0.039 m^3 m^{-3}) and bias (0.020 m^3 m^{-3}) of θ_{HP} from the ILS model. Thus, the new sensor provided satisfactory θ_{HP} results, and a greater accuracy was achieved with the ICPC model than with the ILS model.

Larger deviations of θ_{HP} from θ were observed for the intact soils than for the disturbed soils (Fig. 4). The disturbed samples were packed uniformly, while the intact samples probably had non-uniform soil structure.

Thermo-TDR Bulk Density, Total Porosity, and Air-Filled Porosity

On the five soils, the new thermo-TDR sensor provided ρ_b results that generally agreed with the oven-dry values (Fig. 6), with a RMSE of 0.105 Mg m^{-3} and a bias of -0.017 Mg m^{-3}. Previous studies on laboratory samples reported that the RMSE of thermo-TDR-derived ρ_b values was in the range of 0.134 to 0.178 Mg m^{-3} with either C-based or λ-based methods (Ochsner et al., 2001a; Ren et al., 2003a; Lu et al., 2016; Tian et al., 2018). Apparently, the new sensor and the combined analysis method are effective in improving ρ_b measurement accuracy.

The sensor-estimated n values and the actual n values agreed well, with a RMSE of 0.039 and a bias of 0.003 (Fig. 7a). The n_a values derived from the new thermo-TDR sensor measurements agreed well with the actual n_a values, with a RMSE of 0.035 and a bias of 0.007 (Fig. 7b). Ochsner et al. (2001a) and Ren et al. (2003a) reported RMSEs of about 0.050 for n_a values determined with previous thermo-TDR sensors, which is slightly larger than the results obtained here. Thus, with accurate thermal property and θ measurements, the new thermo-TDR sensor provided relatively accurate ρ_b, n, and n_a values.

Source of Errors

The potential error sources with the new sensor include heat-induced water and vapor redistribution in the soil sample, probe deflections at insertion, and thermal instability under field applications. To minimize thermal-induced water and vapor movement in the soil while obtaining a clear heat pulse signal at the sensing probe, it is critical to regulate the heat pulse strength applied to the heater probe. An optimum heating scheme is obtained by doing a series of tests in agar solution and on repacked soil cores at various water contents (Supplemental Fig. S2 and S3). For this purpose, it is recommended to record the temperatures of both heater and
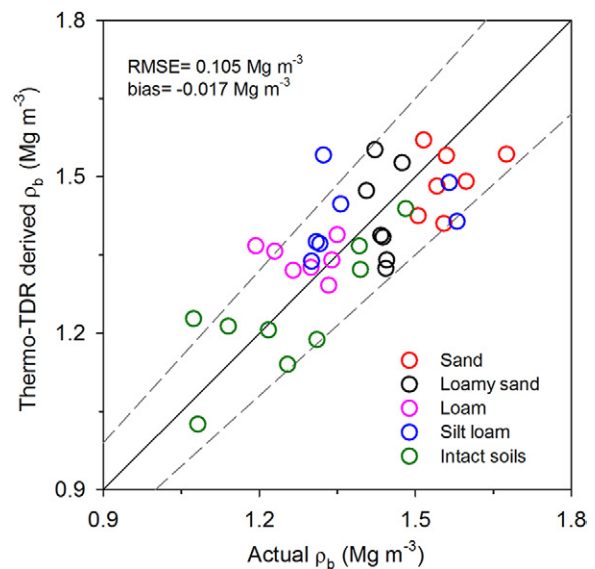

Fig. 6. New thermo-time domain reflectometry (TDR) estimates of soil bulk density (ρ_b) vs. the oven-dried ρ_b values. The solid line is the 1:1 line and the dashed lines are $\pm 10\%$ error lines.
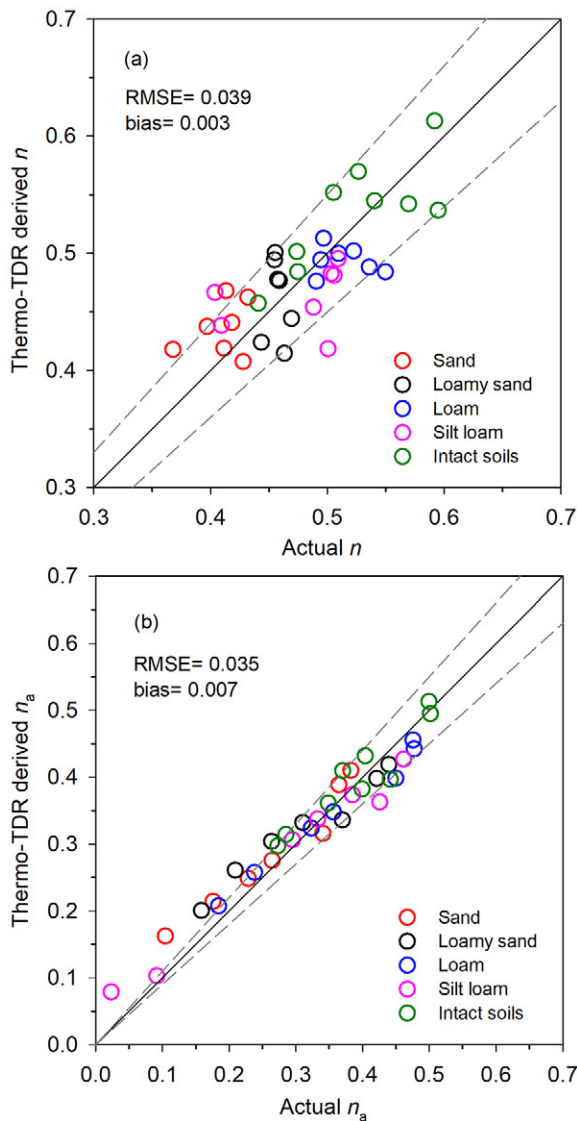
Fig. 7. Thermo-time domain reflectometry (TDR) sensor derived (a) total porosity (n) and (b) air-filled porosity (n_a) vs. actual values. The solid line is the 1:1 line and the dashed lines are ±10% error lines.

previous sensor. The sensing volume of the new sensor is almost three times that of the previous sensor. The ICPC and TL-BMO theories were used to analyze the heat pulse data and TDR waveforms, respectively. Laboratory tests on disturbed and intact soil cores demonstrated that the new sensor provided greater accuracy in thermal property and θ values than did the previous thermo-TDR sensor. The average RMSEs of θ, ρ_b, and n from the new sensor were 0.014 $m^3 m^{-3}$, 0.105 Mg m^{-3}, and 0.039, respectively. Due to improved probe rigidity and greater sensing volume and measurement accuracy, the new thermo-TDR sensor has the potential to monitor θ, thermal properties, ρ_b, n, and n_a in situ.

References

Basinger, J.M., G.J. Kluitenberg, J.M. Ham, J.M. Frank, P.L. Barnes, and M.B. Kirkham. 2003. Laboratory evaluation of the dual-probe heat-pulse method for measuring soil water content. Vadose Zone J. 2:389–399. doi:10.2136/vzj2003.3890

Blackwell, H.H. 1956. The axial-flow error in the thermal-conductivity probe. Can. J. Phys. 34:412–417. doi:10.1139/p56-048

Bristow, K.L., G.J. Kluitenberg, and R. Horton. 1994. Measurement of soil thermal properties with a dual-probe heat-pulse technique. Soil Sci. Soc. Am. J. 58:1288–1294. doi:10.2136/sssaj1994.03615995005800050002x

Campbell, G.S. 1985. Soil physics with BASIC: Transport models for soil–plant systems. Elsevier, Amsterdam.

de Vries, D.A. 1963. Thermal properties of soils. In: W.R. Van Wijk, editor, Physics of plant environment. North-Holland Publ., Amsterdam. p. 210–235.

He, H., M.F. Dyck, R. Horton, T. Ren, K.L. Bristow, J. Lv, and B. Si. 2018. Development and application of the heat pulse method for soil physical measurements. Rev. Geophys. 56:567–620. doi:10.1029/2017RG000584

Heitman, J.L., R. Horton, T.J. Sauer, and T.M. DeSutter. 2008. Sensible heat observations reveal soil water evaporation dynamics. J. Hydrometeorol. 9:165–171. doi:10.1175/2007JHM963.1

Gee, G.W., and D. Or. 2002. Particle-size analysis. In: J.H. Dane and G.C. Topp, editors, Methods of soil analysis. Part 4. Physical methods. SSSA Book Ser. 5. SSSA, Madison, WI. p. 255–294. doi:10.2136/sssabookser5.4.c12

Ghezzehei, T.A. 2008. Errors in determination of soil water content using time domain reflectometry caused by soil compaction around waveguides. Water Resour. Res. 44:W08451. doi:10.1029/2007WR006502

Kamai, T., G.J. Kluitenberg, and J.W. Hopmans. 2015. A dual-probe heat-pulse sensor with rigid probes for improved soil water content measurement. Soil Sci. Soc. Am. J. 79:1059–1072. doi:10.2136/sssaj2015.01.0025

Kamai, T., A. Tuli, G.J. Kluitenberg, and J.W. Hopmans. 2008. Soil water flux density measurements near 1 cm d^{-1} using an improved heat pulse probe design. Water Resour. Res. 44:W00D14. doi:10.1029/2008WR007036

Kluitenberg, G.J., K.L. Bristow, and B.S. Das. 1995. Error analysis of the heat pulse method for measuring soil heat capacity, diffusivity, and conductivity. Soil Sci. Soc. Am. J. 59:719–726. doi:10.2136/sssaj1995.03615995005900030013x

sensor probes. Furthermore, a sensor with a large diameter may be affected by the end effects resulting from a finite probe length, which requires further quantitative investigation, e.g., a simulation study that quantifies the errors of end effects, axial heat flow, as well as the probe–soil interface heat flow. Finally, we tested the new sensor on only a limited number of soil types with clay contents <20%. Future studies are required to test the sensor performance under field conditions and on soils with relatively large clay and organic matter contents.

Conclusions

We introduced a new thermo-TDR sensor to measure soil thermal properties and θ directly, and then derived ρ_b, n, and n_a from the thermal property θ values. The new sensor has longer and more rigid probes and a larger probe-to-probe spacing than the

Knight, J.H. 1992. Sensitivity of time domain reflectometry measurements to lateral variations in soil water content. Water Resour. Res. 28:2345–2352. doi:10.1029/92WR00747

Knight, J.H., W. Jin, and G.J. Kluitenberg. 2007. Sensitivity of the dual-probe heat-pulse method to spatial variations in heat capacity and water content. Vadose Zone J. 6:746–758. doi:10.2136/vzj2006.0170

Knight, J.H., G.J. Kluitenberg, T. Kamai, and J.W. Hopmans. 2012. Semi-analytical solution for dual-probe heat-pulse applications that accounts for probe radius and heat capacity. Vadose Zone J. 11(2). doi:10.2136/vzj2011.0112

Liu, G., M. Wen, X. Chang, R. Horton, and T. Ren. 2013. A self-calibrated DPHP sensor for in situ calibrating the probe spacing. Soil Sci. Soc. Am. J. 77:417–421. doi:10.2136/sssaj2012.0434n

Liu, X., S. Lu, R. Horton, and T. Ren. 2014. In situ monitoring of soil bulk density with a thermo-TDR sensor. Soil Sci. Soc. Am. J. 78:400–407. doi:10.2136/sssaj2013.07.0278

Liu, X., T. Ren, and R. Horton. 2008. Determination of soil bulk density with thermo-time domain reflectometry sensors. Soil Sci. Soc. Am. J. 72:1000–1005. doi:10.2136/sssaj2007.0332

Lu, S., T. Ren, Y. Gong, and R. Horton. 2007. An improved model for predicting soil thermal conductivity from water content. Soil Sci. Soc. Am. J. 71:8–14. doi:10.2136/sssaj2006.0041

Lu, Y., R. Horton, and T. Ren. 2018. Simultaneous determination of soil bulk density and water content: A heat pulse-based method. Eur. J. Soil Sci. 69:947–952. doi:10.1111/ejss.12690

Lu, Y., X. Liu, J.L. Heitman, T. Ren, and R. Horton. 2016. Determining soil bulk density with thermo-time domain reflectometry: A thermal conductivity based approach. Soil Sci. Soc. Am. J. 80:48–54. doi:10.2136/sssaj2015.08.0315

Lu, Y., X. Liu, M. Zhang, J.L. Heitman, R. Horton, and T. Ren. 2017. Thermo-time domain reflectometry method: Advances in monitoring in situ soil bulk density. Methods Soil Anal. 2. doi:10.2136/msa2015.0031

Lu, Y., S. Lu, R. Horton, and T. Ren. 2014. An empirical model for estimating soil thermal conductivity from texture, water content, and bulk density. Soil Sci. Soc. Am. J. 78:1859–1868. doi:10.2136/sssaj2014.05.0218

Lu, Y., Y.J. Wang, and T. Ren. 2013. Using late time data improves the heat-pulse method for estimating soil thermal properties with the pulsed infinite line source theory. Vadose Zone J. 12(4). doi:10.2136/vzj2013.01.0011

Mori, Y., J.W. Hopmans, A.P. Mortensen, and G.J. Kluitenberg. 2003. Multi-functional heat pulse probe for the simultaneous measurement of soil water content, solute concentration, and heat transport parameters. Vadose Zone J. 2:561–571. doi:10.2136/vzj2003.5610

Noborio, K. 2001. Measurement of soil water content and electrical conductivity by time domain reflectometry: A review. Comput. Electron. Agric. 31:213–237. doi:10.1016/S0168-1699(00)00184-8

Ochsner, T.E., R. Horton, and T. Ren. 2001a. Simultaneous water content, air-filled porosity, and bulk density measurements with thermo-time domain reflectometry. Soil Sci. Soc. Am. J. 65:1618–1622. doi:10.2136/sssaj2001.1618

Ochsner, T.E., R. Horton, and T. Ren. 2001b. A new perspective on soil thermal properties. Soil Sci. Soc. Am. J. 65:1641–1647. doi:10.2136/sssaj2001.1641

Olmanson, O.K., and T.E. Ochsner. 2008. A partial cylindrical thermo-time domain reflectometry sensor. Soil Sci. Soc. Am. J. 72:571–577. doi:10.2136/sssaj2007.0084

Peng, X., Y. Wang, J.L. Heitman, T.E. Ochsner, R. Horton, and T. Ren. 2017. Measurement of soil-surface heat flux with a multi-needle heat-pulse probe. Eur. J. Soil Sci. 68:336–344. doi:10.1111/ejss.12421

Ren, T., Z. Ju, Y. Gong, and R. Horton. 2005. Comparing heat-pulse and time domain reflectometry soil water contents from thermo-time domain reflectometry probes. Vadose Zone J. 4:1080–1086. doi:10.2136/vzj2004.0139

Ren, T., G.J. Kluitenberg, and R. Horton. 2000. Determining soil water content and pore water velocity by a heat pulse technique. Soil Sci. Soc. Am. J. 64:552–560. doi:10.2136/sssaj2000.642552x

Ren, T., K. Noborio, and R. Horton. 1999. Measuring soil water content, electrical conductivity, and thermal properties with a thermo-time domain reflectometry probe. Soil Sci. Soc. Am. J. 63:450–457. doi:10.2136/sssaj1999.03615995006300030005x

Ren, T., T.E. Ochsner, and R. Horton. 2003a. Development of thermo-time domain reflectometry for vadose zone measurements. Vadose Zone J. 2:544–551. doi:10.2136/vzj2003.5440

Ren, T., T.E. Ochsner, R. Horton, and Z. Ju. 2003b. Heat-pulse method for soil water content measurement: Influence of the specific heat of the soil solids. Soil Sci. Soc. Am. J. 67:1631–1634. doi:10.2136/sssaj2003.1631

Robinson, D.A., M. Schaap, S.B. Jones, J.M. Wraith, D. Or, and S.P. Friedman. 2003. A review of advances in dielectric and electrical conductivity measurement in soils using time domain reflectometry. Vadose Zone J. 2:444–475. doi:10.2136/vzj2003.4440

Schwartz, R.C., J.J. Casanova, J.M. Bell, and S.R. Evett. 2014. A reevaluation of time domain reflectometry propagation time determination in soils. Vadose Zone J. 13(1). doi:10.2136/vzj2013.07.0135

Song, Y., J.M. Ham, M.B. Kirkham, and G.J. Kluitenberg. 1998. Measuring soil water content under turfgrass using the dual-probe heat pulse technique. J. Am. Soc. Hortic. Sci. 123:937–941. doi:10.21273/JASHS.123.5.937

Song, Y., M.B. Kirkham, J.M. Ham, and G.J. Kluitenberg. 1999. Dual probe heat pulse technique for measuring soil water content and sunflower water uptake. Soil Tillage Res. 50:345–348. doi:10.1016/S0167-1987(99)00014-8

Tarara, J.M., and J.M. Ham. 1997. Measuring soil water content in the laboratory and field with dual-probe heat-capacity sensors. Agron. J. 89:535–542. doi:10.2134/agronj1997.00021962008900040001x

Tian, Z., J.L. Heitman, R. Horton, and T. Ren. 2015. Determining soil ice contents during freezing and thawing with thermo-time domain reflectometry. Vadose Zone J. 14(8). doi:10.2136/vzj2014.12.0179

Tian, Z., Y.L. Lu, T. Ren, R. Horton, and J.L. Heitman. 2018. Improved thermo-time domain reflectometry method for continuous in-situ determination of soil bulk density. Soil Tillage Res. 178:118–129. doi:10.1016/j.still.2017.12.021

Topp, G.C., J.L. Davis, and A.P. Annan. 1980. Electromagnetic determination of soil water content: Measurements in coaxial transmission lines. Water Resour. Res. 16:574–582. doi:10.1029/WR016i003p00574

Topp, G.C., J.L. Davis, W.G. Bailey, and W.D. Zebchuk. 1984. The measurement of soil water content using a portable TDR hand probe. Can. J. Soil Sci. 64:313–321. doi:10.4141/cjss84-033

Wang, Y., Y. Lu, R. Horton, and T. Ren. 2019. Specific heat capacity of soil solids: Influences of clay content, organic matter and tightly bound water. Soil Sci. Soc. Am. J. 83: 1062–1066. doi:10.2136/sssaj2018.11.0434

Wang, Z., Y. Lu, Y. Kojima, S. Lu, M. Zhang, Y. Chen, and R. Horton. 2015. Tangent line/second-order bounded mean oscillation waveform analysis for short TDR probe. Vadose Zone J. 15(1). doi:10.2136/vzj2015.04.0054

Wang, Z., R. Schwartz, Y. Kojima, Y. Chen, and R. Horton. 2017. A comparison of second-order derivative based models for time domain reflectometry waveform analysis. Vadose Zone J. 16(7). doi:10.2136/vzj2017.01.0014

Wen, M., G. Liu, R. Horton, and K. Noborio. 2018. An in situ probe-spacing-correcting thermo-TDR sensor to measure soil water content accurately. Eur. J. Soil Sci. 69:1030–1034. doi:10.1111/ejss.12718

Xie, X., Y. Lu, T. Ren, and R. Horton. 2018. An empirical model for estimating soil thermal diffusivity from texture, bulk density, and degree of saturation. J. Hydrometeorol. 19:445–457. doi:10.1175/JHM-D-17-0131.1

Yu, X., N. Zhang, A. Pradhan, B. Thapa, and S. Tjuatja. 2015. Design and evaluation of a thermo-TDR probe for geothermal applications. Geotech. Test. J. 38:864–877. doi:10.1520/GTJ20150023

Zhang, X., S. Lu, J.L. Heitman, R. Horton, and T. Ren. 2012. Measuring subsurface soil-water evaporation with an improved heat-pulse probe. Soil Sci. Soc. Am. J. 76:876–879. doi:10.2136/sssaj2011.0052n

An improved thermo-TDR technique for monitoring soil thermal properties, water content, bulk density, and porosity

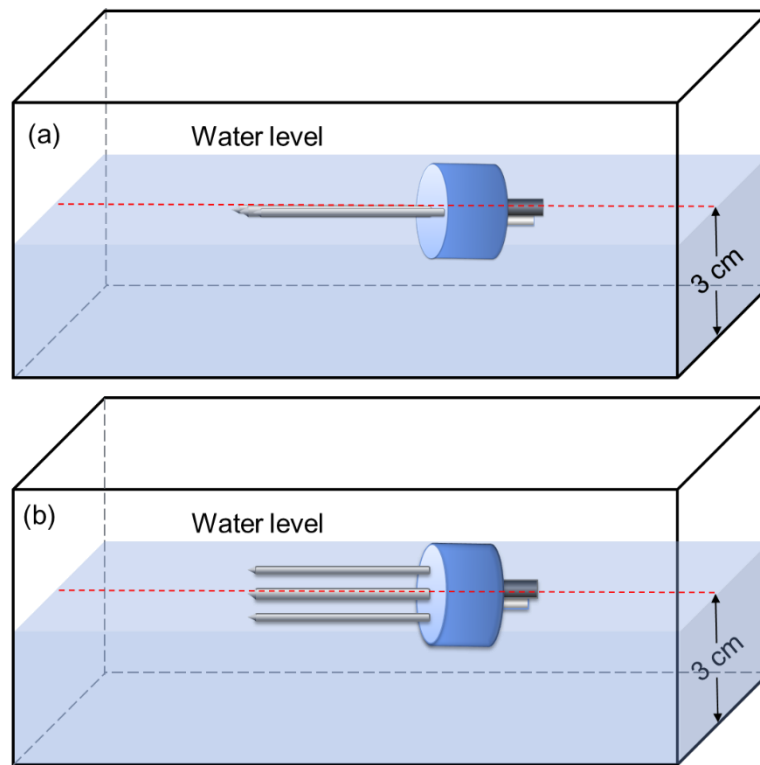*1. The Experimental Setup to Determine the Sensing Volume of the New Thermo-TDR Sensor*

Figure S1. A schematic diagram showing the procedures for determining the sensing volume of thermo-TDR sensors. Two scenarios were considered: (a) the probe plane was parallel to the container bottom (Horizontal position), and (b) the probe plane was vertical to the container bottom (Vertical position). The container was a rectangular glass container 22.5-cm in length, 16-cm in width and 8-cm in height. The red dashed line represents the initial water surface. Additional water was added in 2-mm increments, and TDR waveforms were collected after each water addition.

2. The Observed Values and Parameters Involved in the Thermo-TDR Measurements

To obtain detectable and clear temperature signals, a large amount of heat compared to that used with the early sensors is introduced to the soil, because of the

larger probe body and spacings of the new sensor. It is important to consider the possible consequences of water and vapor movement due to the thermal gradient created by the heat pulse. Thus, a series of experiments were performed to determine the optimum heat duration to produce an appropriate temperature rise in the sensor and to minimize possible errors caused by water and vapor flow. Figures S2 and S3 show the thermo-TDR measured temperatures in sensor and heater probes, respectively. Table S1 lists the parameter values for the measurements and curve-fitting procedure.
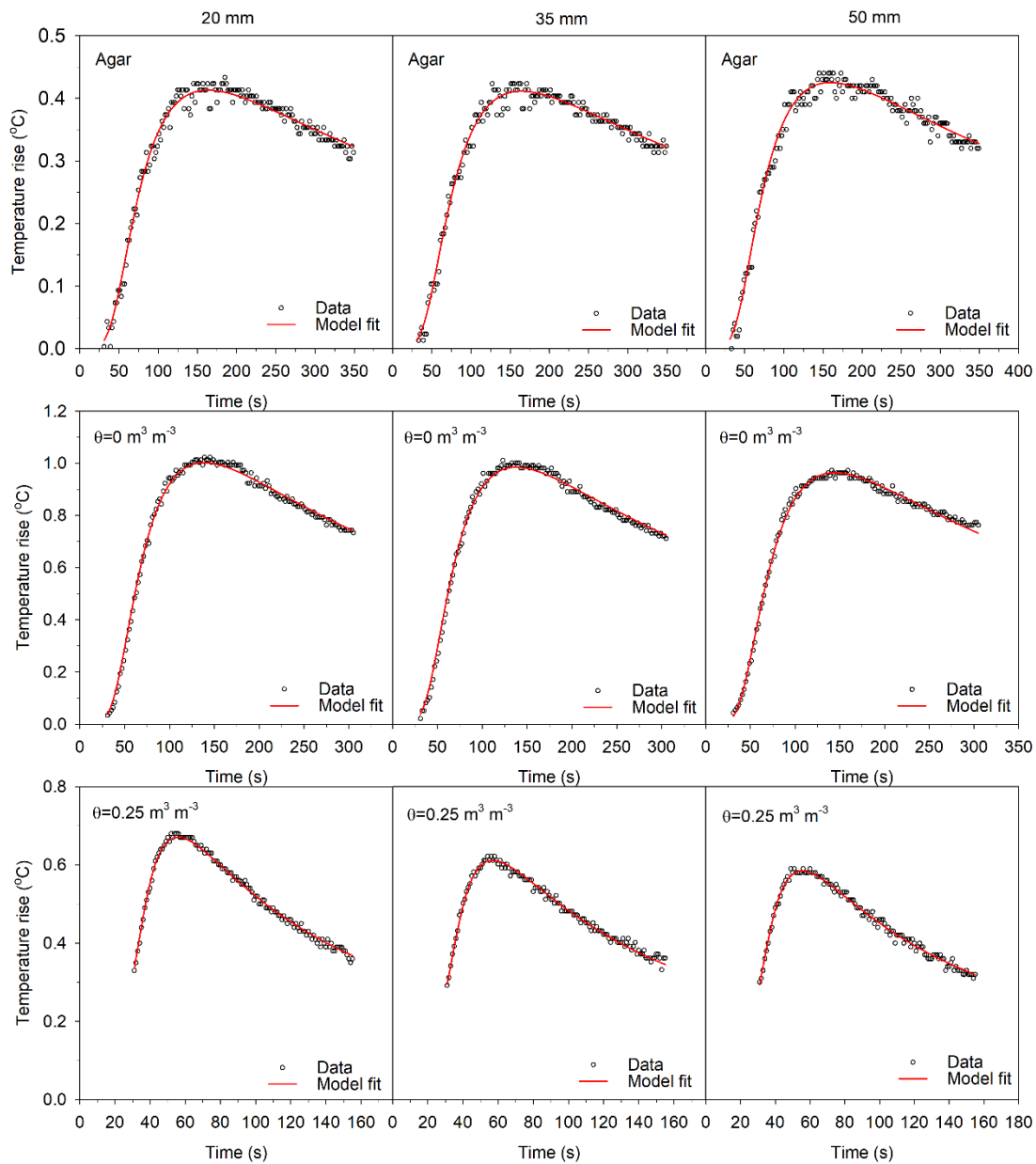

Figure S2. An example dataset of thermo-TDR measured temperature changes (circles) and the fitting results of the identical cylindrical perfect conductors (ICPC) model to the measured data (red lines) on a sand soil at soil water contents

(θ) of 0 and 0.25 m³ m⁻³, and in agar solution (5 g L⁻¹), respectively. The values 20 mm, 35 mm, and 50 mm indicate that data are collected at these three positions in a sensing probe. Table S1 lists the parameters used for curve fitting.

Figure S2 shows typical temperature changes as a function of time in agar solution and soil samples (dry and wet). The maximum temperature rise is lowest for the agar solution (~0.4°C). In the sand soil, the maximum temperature rises are 0.7-1.0°C, depending on soil water content. Additional water in soil increases the soil heat capacity, thus lowering the temperature rise of a heat pulse signal.

Table S1. The key parameters for curve-fitting: heat pulse intensity (q'), probe heat capacity (C_0) and probe radius (a_0) of the new thermo-TDR sensor, the heating duration (t_0) and the time range for the curve fitting (t_f). The values for the above parameters correspond to the data presented in Fig. S2.

Parameters	Agar solution	Soil samples	
		$\theta = 0$ m³ m⁻³	$\theta = 0.25$ m³ m⁻³
q' (W m⁻¹)[¶]	47.13	47.04	47.12
C_0 (MJ m⁻³ K⁻¹)		3.68[§]	
a_0 (m)		0.00119	
t_0 (s)	30	25	25
t_f (s)	31−350	31−300	31−150

[§] This value is calculated based on the equation proposed by Knight et al. (2012) for estimating the heat capacity of heat pulse probes (Eq. [42] in the Knight et al. (2012) paper). The values for the heat capacities of the epoxy and stainless steel are 2.03 and 4.00 MJ m⁻³ K⁻¹, respectively, according to Kamai et al. (2015).

[¶] q' is calculated from the resistance and the current in the heater wire.

Table S1 lists the values of parameters used for fitting the model to measured data (Fig. S2). Considering the relatively large probe spacing (~10 mm) for the new thermo-TDR sensor, a heat intensity of about 47 W m⁻¹ with a long heating time (25-30 s) was used to make sure the temperature rise at the sensing probe was between 0.4 and 1.0°C.

The time length used for the curve-fitting is also listed in Table S1. To reduce the potential errors from the finite probe properties, the time length of temperature change data used for curve fitting should be carefully considered. If the temperature response curve has a flat peak (e.g., on a dry soil or in agar solution), the temperature data within

300-350 s are recommended (Fig. S2). When the temperature response curves have a well-defined peak (e.g., on wet soils), the data within the time range of 150 s are recommended.
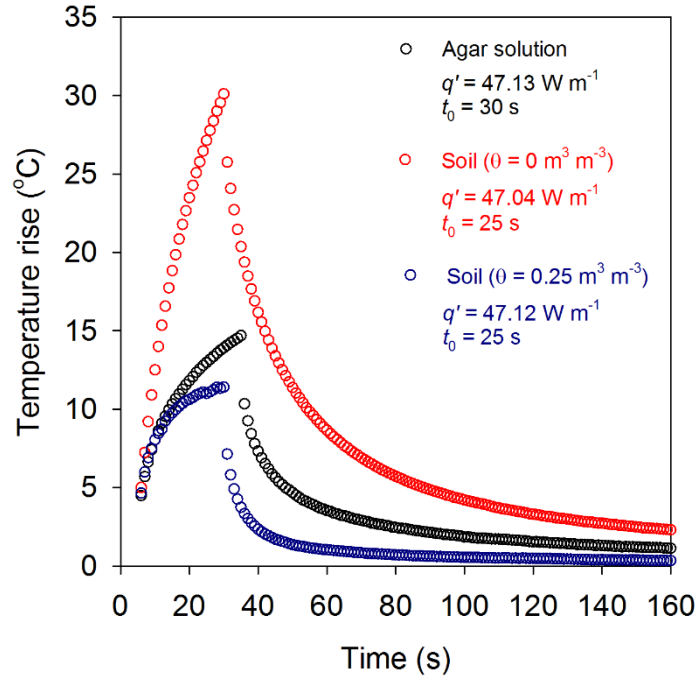

Figure S3. Temperature rise dynamics at the heater probe during the heat pulse measurement. Parameter θ represents soil water content, t_0 and q' represent the time duration and heating rate of the heat pulse measurement, respectively. The example datasets were collected on a sand soil at water content (θ) of 0 and 0.25 m^3 m^{-3}, and in an agar solution (5 g L^{-1}).

The results show that the maximum temperature rises at the heater probe can reach 30°C in dry soils and 15°C in the agar solution (Fig. S3). The heating intensity should be carefully regulated to minimize the effects of water and vapor migration under thermal gradients in soil, and to obtain detectable and clear temperature signals, because of the relatively large probe spacings of the new sensor.

3. Sensor Overview

The thermo-TDR sensor directly measures state variables of soil temperature and TDR waveform. From these measurements, soil thermal properties and θ are determined, and ρ_b, n and n_a are estimated based on the functional relationships between soil thermal properties and particle-size distribution, θ, and ρ_b. Figure S4 illustrates the

variables, parameters and estimation methods included in the thermo-TDR technique for determining soil physical properties.
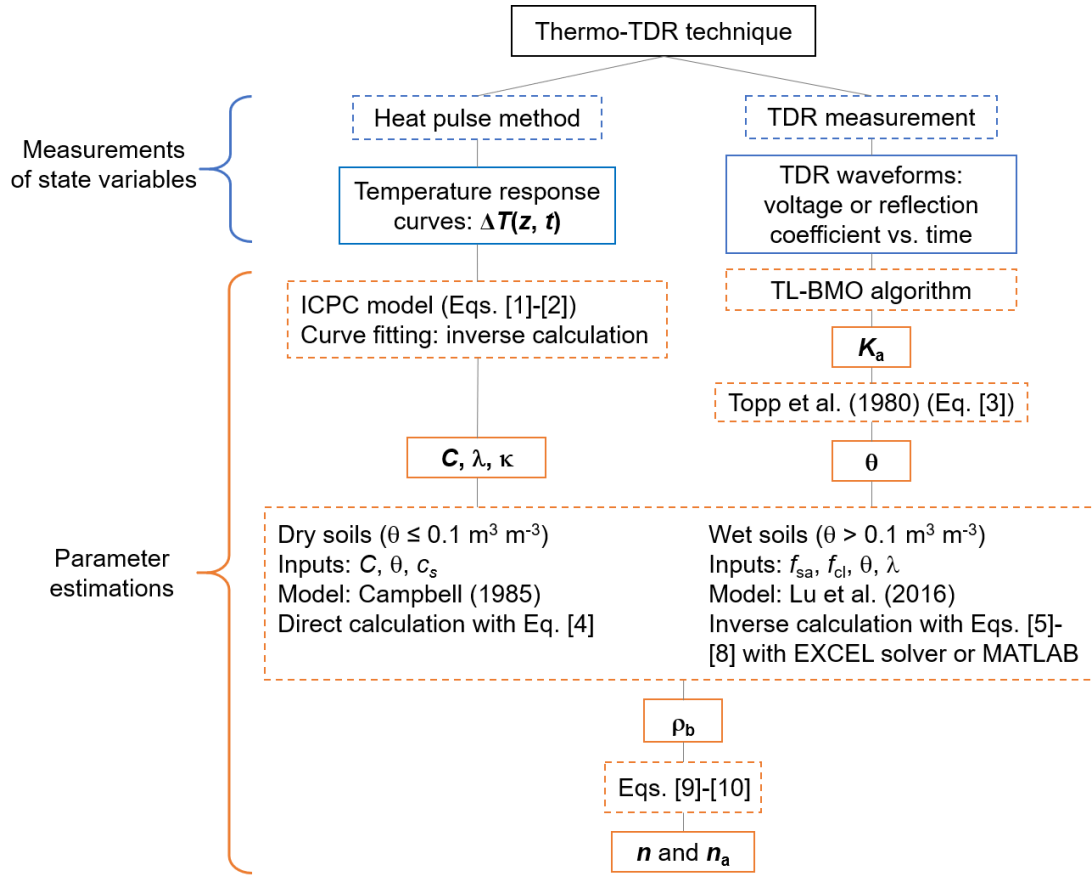

Figure S4. An overview diagram for the thermo-TDR sensor to determine soil thermal properties, water content (θ), bulk density (ρ_b), porosity (n), and air-filled porosity (n_a). K_a, C, λ, c_s, f_{sa}, and f_{cl} represent soil dielectric constant, volumetric heat capacity, thermal conductivity, specific heat capacity of soil solids, the fractions of sand and clay, respectively. The dashed-line text box represents the 'methods and calculations', and the solid-line text box represents the 'measured or the estimated variables/parameters'.